Archaeological Prospection

WILEY

RESEARCH ARTICLE OPEN ACCESS

Integrated Electromagnetic Mapping Through K-Means to Improve Identification of Areas of Archaeological Interest

Angelica Capozzoli[1] | Valeria Paoletti[1,2] | Federico Cella[3] | Mauro La Manna[1] | Ester Piegari[1]

[1]Department of Earth, Environmental and Resources Sciences, University of Naples Federico II, Naples, Italy | [2]Istituto Nazionale di Geofisica e Vulcanologia – Sezione di Napoli Osservatorio Vesuviano, Naples, Italy | [3]School of Sciences and Technologies, Geology Division, University of Camerino, Camerino, Italy

Correspondence: Valeria Paoletti (paoletti@unina.it)

Received: 13 February 2025 | **Revised:** 16 April 2025 | **Accepted:** 20 May 2025

Funding: The authors received no specific funding for this work.

Keywords: archaeogeophysics | FDEM data | Iron Age | *K*-means integrated EM maps | Torre Galli

ABSTRACT

This study proposes a procedure to improve the interpretation of data from the Frequency Domain ElectroMagnetic method (FDEM), a geophysical technique with high benefit–cost ratios in archaeology. This method enables the simultaneous analysis of electrical and magnetic properties of the investigated medium, providing data as in-phase and out-of-phase (quadrature) components of the electromagnetic field. Traditionally, FDEM produces individual maps for these components that are typically inspected and related to each other only visually. The proposed procedure is based on unsupervised machine learning that, by providing integrated maps of these two components, overcomes the limitations of visual inspection and streamlines the interpretative phase. The FDEM data acquired at the Torre Galli archaeological site in Calabria, Italy, were clustered using *K*-means, known for its effectiveness in partitioning densely distributed spatial data. The optimal number of clusters was determined through silhouette analysis. Once identified, the clusters were classified as either representative of the natural background or indicative of archaeological interest and mapped in real space. This analysis identified several areas with anomalous geophysical characteristics compared to the natural context, characterized by distinct ranges of EM property values, suggesting the presence of different archaeological targets, such as road, walls and iron/bronze tools, which are distributed heterogeneously in the subsoil. This classification facilitated the rapid delineation of areas with significant archaeological potential that may warrant further investigation, resulting in a reduction of both the study area size and the archaeological effort associated with excavation. A comparison of these areas with previous excavations and the results of a magnetic survey shows that the proposed procedure is promising in enhancing the efficiency and accuracy of the FDEM method for identifying areas of archaeological interest. The findings suggest a move towards automation in the interpretation process, which could improve cost-effectiveness and time optimization in geophysical and archaeological investigations.

1 | Introduction

The use of geophysics in archaeology has made considerable progress in recent years, allowing the detection of buried materials dating back to ancient human activities. By using geophysical methods, archaeologists can improve their understanding of archaeological sites and ensure the preservation of cultural heritage for future generations (e.g., Piro 2008; Cozzolino et al. 2018; El-Qady and Metwaly 2018; Martorana et al. 2023 and references therein).

In the literature, there are various applications of geophysical methods to the archaeological field. The purposes can be multiple, and some examples of applications aim to (i) study the distribution of targets in the subsoil of known sites, guiding targeted excavations, through the use of single methods, typically the magnetic method (e.g., Paoletti et al. 2005; Fedi et al. 2017; Florio et al. 2019) or through multimethodological geophysical investigations (e.g., Carrara et al. 2001; Di Maio et al. 2018; Casas et al. 2022; Grassi et al. 2023); (ii) confirm the existence of hypothesized archaeological sites and targets, providing valuable data for further investigation and preservation efforts (e.g., Soupios et al. 2013; Cella et al. 2015; Bianco et al. 2024; Paoletti et al. 2024); and (iii) evaluate the state of conservation of underground archaeological assets (e.g., Milo et al. 2022 and references therein).

Among the geophysical prospecting methods, the Frequency Domain ElectroMagnetic method (FDEM) has become a valuable tool for archaeologists over the last decades, as it allows fast and noninvasive exploration of larger areas while reducing the costs associated with excavation campaigns (e.g., Boschi 2020; Sea and Ernenwein 2021; Deiana et al. 2022; Rizzo et al. 2023).

EM instruments are frequently used for archaeological work because they are lightweight and mobile and do not require contact with the ground and because they enable the simultaneous recording of both the electrical and magnetic properties of the soils (e.g., Tabbagh 1986; Gaffney et al. 2002; De Smedt et al. 2013). FDEM involves generating an electromagnetic field oscillating between 1 and 100 kHz using a transmitter coil (Tx), which induces eddy currents in conductive soil. These eddy currents create a secondary electromagnetic field that generates an oscillating current in the receiver coil (Rx). The receiver detects this secondary field and separates it into two components. The first component is the in-phase component, which is aligned with the primary signal and measured in parts per thousand (ppt). The second component is the quadrature component, which is 90° out of phase with the primary signal and is typically output in millisiemens per metre (mS m^{-1}) using an approximate function. Typically, the outcomes of a FDEM prospection are spatial maps of the individual EM component values that provide insights into the magnetic and electrical properties of the investigated subsurface separately.

Although some procedures have been recently proposed for the inversion of FDEM data (e.g., Benech et al. 2016; Christiansen et al. 2016; Deidda et al. 2020; Narciso et al. 2025), the interpretation of FDEM data is still primarily based on the visual inspection and correlation of the EM maps. This study aims to contribute to improving the interpretative process by developing a procedure (illustrated in Figure 1) that integrates data from both the EM components in a way that reduces the inherent subjectivity of visual inspection while simultaneously moving towards an automation of the interpretative process.

Utilizing a partitional cluster analysis, the *K*-means algorithm, data groups characterized by specific intervals of the in-phase and quadrature components were identified, and integrated EM maps were obtained. These maps show the study area automatically divided into subareas with specific ranges of physical properties being considered. The subsequent identification of subareas with potential archaeological interest is then an essentially semiautomatic process, guided by the operator's geological and archaeological knowledge of the site.

Specifically, FDEM data were clustered in the parameter space, and the optimal number of clusters was searched for from the silhouette analysis. Once clusters were identified, they were mapped back into real space, and areas of potential archaeological interest that warrant further studies were identified.

The paper is organized as follows. Section 2 describes the archaeological site of Torre Galli and is divided into two subsections providing information on geological/archaeological setting and on geophysical surveys. Section 3 illustrates the procedure proposed to generate integrated maps of the EM components and is divided into three subsections, which describe (i) data characteristics and normalization, (ii) *K*-means algorithm and (iii) the used clustering validation methods. Section 4 shows the results of the cluster analysis, which are discussed and compared with those from a magnetic study in Section 5. Section 6 outlines the conclusions.

2 | Torre Galli Site

Torre Galli is an archaeological site located on the western edge of Monte Poro plateau in Calabria, Italy (Figure 2a). This site was selected for its notable archaeological importance, particularly during the Iron Age.

2.1 | Geological and Archaeological Setting

Geologically, the archaeological site is located over marine sediments of Tortonian age, lying above a crystalline basement (Tortorici et al. 2003). These sediments are characterized by arenaceous deposits with a predominant carbonate fraction towards the top (Nicotera 1959; Rao et al. 2007; Gramigna et al. 2008; Calcaterra and Parise 2010). In the study area, this succession has a hypothesized thickness of between 5 and 20 m, based on references from nearby outcrops (Ietto and Ietto 2004).

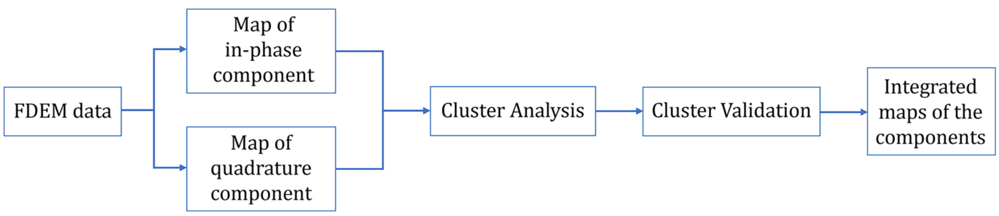

FIGURE 1 | Scheme of the proposed procedure for automatization of FDEM data integration.

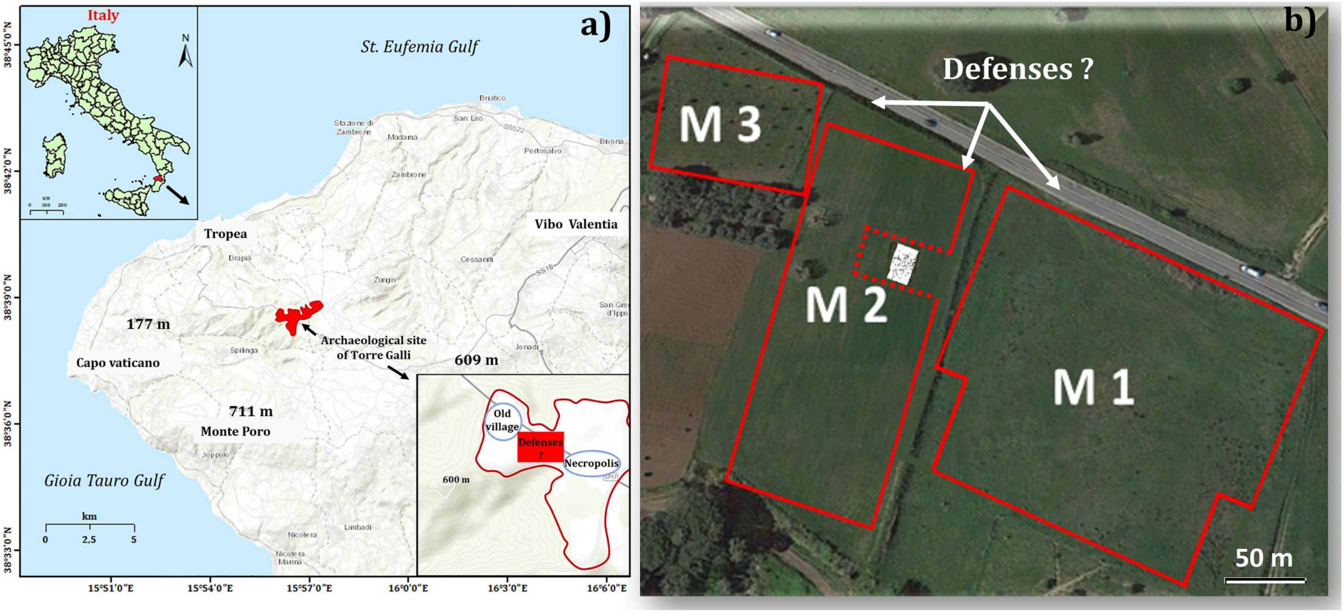

FIGURE 2 | (a) Geographical map showing the area where the archaeological site of Torre Galli is located (red filled area); bottom right: settlement of the site; the red rectangle (defences?) points out the area of this study; (b) enlargement of the defence zone (red filled rectangle in a): meshes M1–M3 of the geophysical survey. The white rectangle in M2 is the excavation prior to the 2012 campaign, which highlighted the presence of a ditch.

Torre Galli is placed at an altitude of approximately 620 m above sea level (a.s.l.), on a marine terrace (Figure 2a). This strategic position allowed it to oversee a vast and resource-rich area. Recognized as one of Italy's most significant archaeological sites for the Iron Age studies, Torre Galli has attracted the interest of numerous archaeologists since the early twentieth century (Pacciarelli 1999; Orsi 2004). The site is believed to have played a crucial role as a transit point within a trade network that extended across the entire Mediterranean (Orsi 1926).

Initial excavations conducted by Orsi (1926, 2004) between 1922 and 1923 uncovered extensive necropolises and settlement traces, revealing a wealth of artefacts that highlight the site's historical importance. The discovery of a necropolis with 280 burial pits, dated to the Iron Age, suggests the presence of a thriving indigenous community, populated by 400–600 people, from the 9th and to the 8th century BC. Near the necropolis, Orsi uncovered evidence of habitations in the form of huts, which were further supported by a significant number of earthenware and ceramic fragments primarily dating back to the 6th century BC. A comprehensive analysis of the tomb types, grave goods and burial practices, typically involving inhumation in rectangular or elliptical pits adorned with rich metal and ceramic items, led Orsi to propose that the necropolis was utilized from the 10th to the 6th century BC (Orsi 1926, 2004; Benelli 2012; Abbate 2014).

However, the absence of materials from the 8th and 7th centuries BC among Orsi's excavation findings prompted a reevaluation of the chronological framework. This led to the identification of two distinct phases of use for the necropolis: a first phase, associated with the Early Iron Age, concluded around the mid-8th century BC and characterized by impasto pottery, double-edged razors, short swords and bow fibulae. The second phase is dated to the first half of the 6th century BC (e.g., La Genière 1964; Benelli 2012).

One notable change between the two phases was the gradual adoption of hand-manufactured iron goods marking a shift in the culture of materials. The role of the male 'warrior' also became more prominent, as shown by a widespread presence of personal iron armaments. This period marked a stronger differentiation among social and economic classes, transitioning from a dominant warrior aristocracy to a society characterized by large landowner families with their own military organizations (e.g., Cella and Fedi 2015; Bettelli and Vagnetti 2019).

This hypothesis was supported by subsequent excavation campaigns conducted by Pacciarelli (Pacciarelli et al. 2017), which identified the remains of stone walls with regular geometry and traces of a fireplace, confirming the presence of a community deeply engaged in military activities. These findings suggested that the Monte Poro plateau was probably suitable for hosting a more developed village, especially considering its natural barriers. The plateau is bordered to the east by the necropolis and defended by steep slopes on the southern, western and northern sides, with access only limited to the eastern side. Archaeologists hypothesize that during the Early Iron Age, Torre Galli had a defensive system along its eastern side, approximately 250 m wide, situated between the village and the necropolis (inset in Figure 2a). This system likely consisted of ditches associated with stone structures, such as small walls and/or roads.

There is evidence (Pacciarelli et al. 2017) that such ditches were filled during the Early Iron Age, perhaps in conjunction with fire events. Indeed, excavations at Torre Galli have revealed that the areas with the finds of major interest (masonry structures and/or road pavements) bear evident and widespread traces of fire. These traces are witnessed by the presence of abundant burnt soil, of charred wooden material (poles and beams), together with many bricks calcined by fire. Downstream of the potential main moat and parallel to it, a trench approximately 1 m wide, dug into the rock was identified (see M2 area in Figure 2b). These remains could belong to a 6th century structure associated with this defensive system (Pacciarelli et al. 2017).

The amount of information provided by the previous archaeological digs confirmed the need for new excavations between the necropolis and the old village. However, the large area affected by the hypothesized defensive structures has made the prospect of further digging challenging. For this reason, in 2012, a geophysical investigation was carried out in the area shown in Figure 2b (Cella and Fedi 2015).

2.2 | Geophysical Survey

In the summer of 2012, a high-resolution geophysical survey was conducted at Torre Galli to identify and locate buried archaeological defence structures (Cella and Fedi 2015). The survey covered approximately 14 400 m^2 at elevations ranging from 605 to 615 m a.s.l. Due to its size, the area was divided into three sectors (M1–M3) for separate investigations (Figure 2b). The geophysical investigation employed magnetic and electromagnetic methods chosen on the basis of the physical characteristics of the hypothesized archaeological targets including walls, roads, ditches, furnaces, accumulations of fired artefacts and iron/bronze artefacts. These materials typically exhibit a magnetic susceptibility higher than the surrounding environment, when embedded in a sandstone subsoil. Furthermore, these targets exhibit electrical conductivity characteristics that differ from that of the natural background. Typically, more compact and less porous materials (such as the bricks of walls and roads) have lower electrical conductivity compared to a more porous and less compact arenaceous subsoil. On the other hand, metallic objects are generally characterized by significantly higher electrical conductivity than both arenaceous subsoils and bricks.

The FDEM data were collected using a GSSI PROFILER EMP-400, a multifrequency EM induction tool. This sensor is characterized by a fixed separation of 1.21 m between the transmitter and the receiver coils, generally kept 20 cm above the ground level. This instrument can analyse up to three different frequencies simultaneously, ranging from 1 to 16 kHz. For this study, the three frequencies of 15, 10 and 5 kHz were selected, in vertical mode configuration, to accurately explore the upper few metres of the subsurface.

Estimating the exploration depth of an EM measurement system is complex due to factors such as coil orientation, coil separation, measurement frequency and the electromagnetic properties of the soil (Reynolds 2011; Saey et al. 2012). This work follows the findings of Cella and Fedi (2015), which indicate a detection depth range of approximately 0–3 m, compatible with the expected depth of the investigated targets and supported by magnetic data analysis.

Data (the quadrature and in-phase components) were acquired along equidistant profiles at a sampling rate of two to three measures per second with a transect spacing of 1 m. The EM data were georeferenced using a Leica Geosystem differential GPS with centimetric precision in the UTM WGS84 coordinate system, alongside aerial images and a digital terrain model (DTM) of the area. The acquired FDEM data (Figure 3) were processed to reduce noise and highlight key archaeological features. For detailed processing steps, please refer to Cella and Fedi (2015).

3 | Building the Integrated EM Maps

Looking at Figure 3, it is clear that the visual inspection of the EM maps leaves room for ambiguities in data interpretation. The identification of areas characterized by the highest and/or

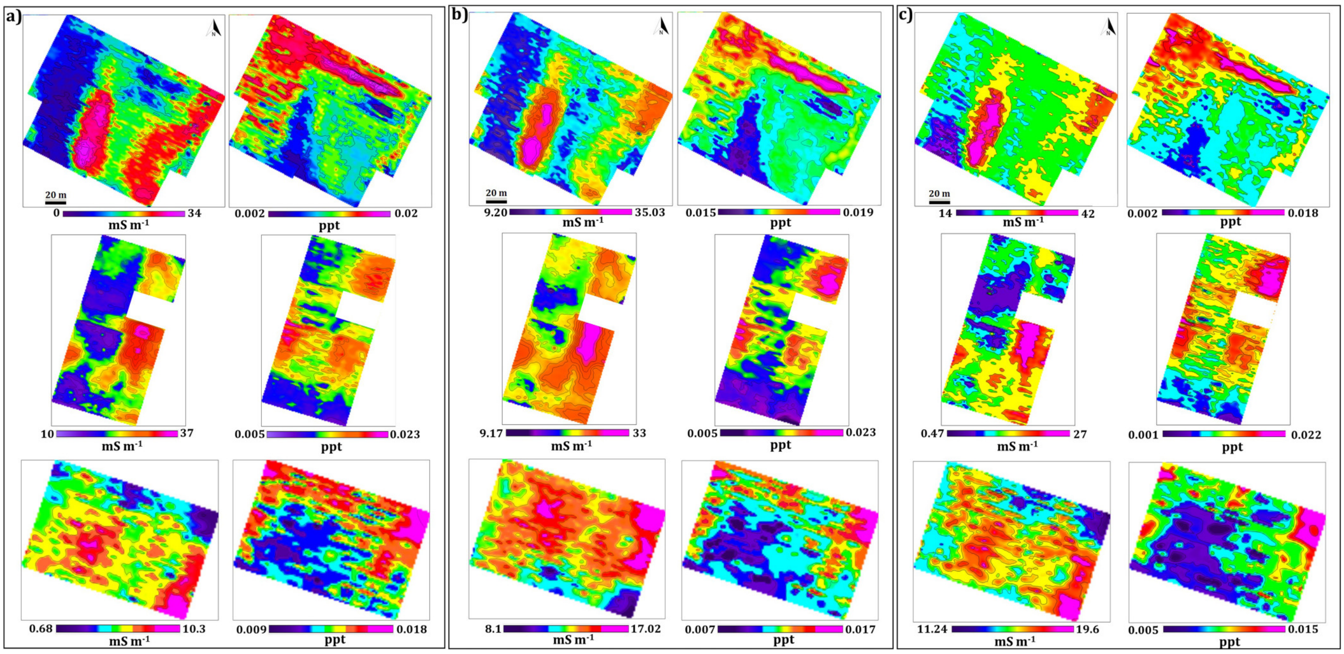

FIGURE 3 | Maps of the quadrature and in-phase components (left and right of each panel), after the processing phase, acquired for the three acquisition frequencies 5 kHz (a), 10 kHz (b) and 15 kHz (c) in the three meshes of the survey (M1–M3 from top to bottom).

lowest values of the EM components is influenced by the choice of colour scale. Consequently, the size and the shape of the areas of potential interest are not identified objectively and univocally. In this section, the steps of the procedure developed to overcome this issue and generated integrated EM maps are described.

3.1 | Data Characterization and Normalization

The dataset analysed in this study has been assembled starting from the FDEM data shown in Figure 3. The dataset consists of nine matrices, with three for each survey area (M1–M3) corresponding to different acquisition frequencies. The total number of datapoints is 28 955 for M1, 18 229 for M2 and 10 808 for M3. Tables 1 and 2 summarize the statistical metrics for each dataset.

The Low Induction Number (LIN) condition is crucial for interpreting FDEM data, as it ensures that the relationship between the primary and secondary magnetic fields remains valid (e.g., Won and Huang 2004; Simon et al. 2015). The concept of LIN condition in the FDEM method is widely attributed to Fraser (1972), who discussed the apparent conductivity approximation under low induction number conditions in frequency-domain electromagnetic systems. Additionally, Wait (1955) and McNeill (1980) contributed to the theoretical foundation of electromagnetic induction and its applications. When this condition is satisfied, the electrical conductivity measurements acquired at different frequencies can provide insights into the subsurface properties at varying depths. To verify this, the induction number N was calculated, defined as the ratio between the intercoil spacing and the skin depth $\delta = 1/\sqrt{\pi \mu_0 \mu_r \sigma f}$. Using $\mu_0 = 4\pi \cdot 10^{-7}$ H/m, $\mu_r = 1$ and the values for electrical conductivity σ and frequency f from Table 1, the condition $N << 1$ is confirmed to hold for all Survey Areas M1–M3.

This was later confirmed by an additional study examining the values of the EM components in the parameter space, which revealed how their distribution varies across different acquisition frequencies (Figure 4).

Notably, M1 and M3 show clear distinctions with minimal overlap in the data acquired at different frequencies (Figure 4a,c). As the frequencies decrease, for both M1 and M3, the values of quadrature components decrease, whereas those of the in-phase components increase. However, for the M1 area, there is a simple shift in the range of values of the two components, whereas for the M3 area, the shape of the value distribution changes significantly with decreasing frequencies.

TABLE 1 | Statistical metrics for the values of the quadrature component.

Mesh	Acquisition frequency	Min (mS m^{-1})	Max (mS m^{-1})	Mean (mS m^{-1})	Std (mS m^{-1})
M1	5 kHz	0.5945	33.2337	11.2967	4.6633
	10 kHz	9.2777	35.0238	17.0425	4.0181
	15 kHz	14.3633	41.5553	24.5385	3.5949
M2	5 kHz	10.1932	36.4208	17.9762	4.4007
	10 kHz	9.1934	32.8222	16.8696	4.5415
	15 kHz	0.0484	26.2452	10.2286	4.5370
M3	5 kHz	0.6867	10.2139	6.1628	1.6050
	10 kHz	8.1254	17.0109	13.1647	1.2804
	15 kHz	11.2440	19.5779	15.7265	1.2382

TABLE 2 | Statistical metrics for the values of the in-phase component.

Mesh	Acquisition frequency	Min (ppt)	Max (ppt)	Mean (ppt)	Std (ppt)
M1	5 kHz	0.0025	0.0200	0.0074	0.0023
	10 kHz	0.0016	0.0184	0.0060	0.0023
	15 kHz	0.0020	0.0175	0.0032	0.0023
M2	5 kHz	0.0050	0.0230	0.0125	0.0029
	10 kHz	0.0053	0.0230	0.0126	0.0029
	15 kHz	0.0010	0.0220	0.0120	0.0027
M3	5 kHz	0.0096	0.0179	0.0125	0.0015
	10 kHz	0.0076	0.0167	0.0109	0.0014
	15 kHz	0.0057	0.0144	0.0085	0.0013

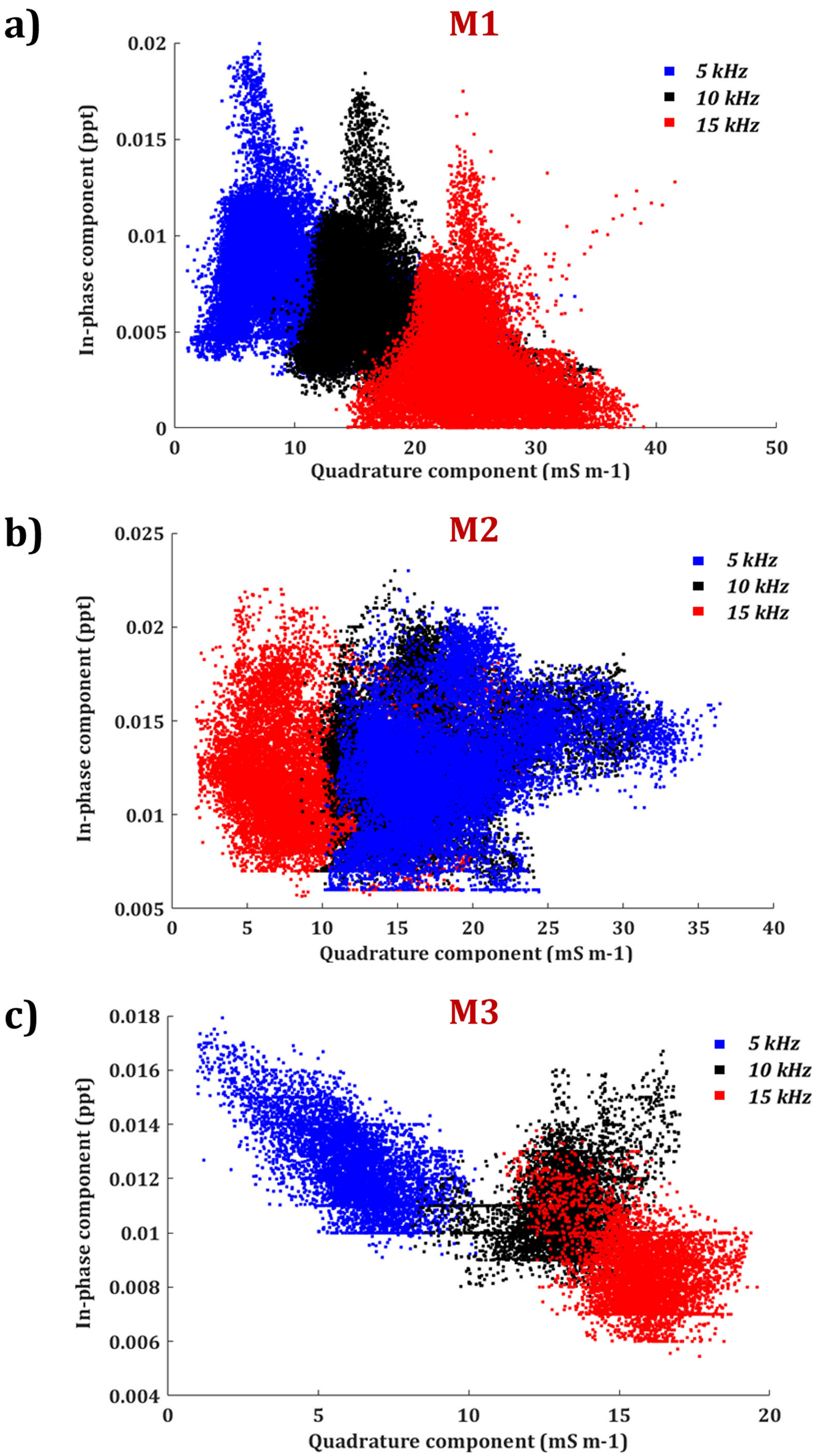

FIGURE 4 | Comparison of in-phase and quadrature component values relative to the different acquisition frequencies for meshes (a) M1, (b) M2 and (c) M3.

The mesh M2 exhibits significant overlap between the 5- and 10-kHz datasets (Figure 4b). In contrast, the 15-kHz frequency data display lower quadrature component values, suggesting the presence of a shallow resistive layer. In the present study, the 5- and 10-kHz datasets were chosen based on the variability observed in Figure 4, to examine if there are significant differences between them. The 15-kHz dataset was instead excluded from cluster analyses due to signal noise issues, as previously reported by Cella and Fedi (2015).

This data representation also shows how the values of the two EM components exhibit significantly different ranges of variation, differing by several orders of magnitude. To ensure that the different scales do not skew the importance of the EM components in clustering, data normalization has been implemented. By scaling the data to a uniform range of 0–1, the impact of disparate data ranges is effectively mitigated, allowing for a more accurate and meaningful analysis. Specifically, the logarithm of the original data is considered and then rescaled to the interval [0, 1] using the following equation:

$$x_{new} = \frac{max(x_{new}) - min(x_{new})}{max(x_{old}) - min(x_{old})}\left(x_{old} - min(x_{old})\right) + min(x_{new}), \tag{1}$$

where x_{old} is the original $\log_{10}$ transformed value of the component and x_{new} is the respective normalized value. Normalization using a logarithmic transformation has the advantage of compressing the range and making the data more normally distributed. This is particularly beneficial when dealing with variables that span several orders of magnitude, as it helps mitigating the influence of outliers.

3.2 | Cluster Analysis Through *K*-Means Algorithm

Over the years, there has been an increasing number of applications of clustering algorithms proposed to improve geological and geophysical data analysis and interpretation (Florio and Lo Re 2018; Bernardinetti and Bruno 2019; Ambrosino et al. 2022, 2023, 2024; Cicchella et al. 2022; Cutaneo et al. 2023; Modabberi et al. 2023; Piegari et al. 2023).

In this work, cluster analysis was conducted using one of the most widely utilized partitional clustering methods: *K*-means. This algorithm was chosen due to its efficiency in clustering large, homogeneous datasets, its straightforward implementation and its relatively quick execution time. This algorithm divides the data within a dataset into *K* predefined, nonoverlapping groups (clusters) based on a similarity measure, typically using Euclidean distance (Murphy 2012). The process begins by choosing the number of clusters, *K*, and then, it randomly assigns the position of *K* points, called centroids (μ_i), in the parameter space. Subsequently, the algorithm calculates the distance between each point and the *K* centroids, assigning each point to the cluster with the closest centroid. An iterative loop then begins, during which the centroid positions are updated as the mean of the points assigned to the previous centroids. The iterative cycle continues until the cost function *E* defined by the following equation is minimized (Bhattacharya 2021):

$$E = \sum_{i=1}^{K} \sum_{n=1}^{N} r_{ni}\left(x_n - \mu_i\right)^2, \tag{2}$$

where x_n denotes the data points, *N* is the total number of points in the dataset and r_{ni} is a binary variable equal to 1 if x_n is assigned to cluster *i* and 0 otherwise.

One of the main drawbacks of K-means is that the algorithm tends to find different local minima of *E* for each different initial position of the centroids, providing different cluster solutions. To face this issue, an iterative cycle was employed on the initial configuration of centroids, enabling the tracking of variance for every initial configuration. Specifically, 50 different starting configurations of the position of centroids were considered, and the cluster solution was chosen as the one corresponding to the lowest variance.

K-means requires as input the number of *K* clusters into which one wants to divide the initial dataset. If this number is unknown, the algorithm is usually applied with different *K*, and the best value for *K* is chosen from one of the various methods of clustering validity proposed in the literature (e.g., Desgraupes 2013).

3.3 | Cluster Validation

In this study, two validation approaches are analysed to measure the quality of clustering: the elbow method and the silhouette coefficient.

The elbow method is classified as a relative cluster validation as it evaluates the clustering results by varying the number of clusters and comparing the different clustering by looking for an 'elbow' in the plot of the within-cluster sum of squares versus the number of clusters (Bhattacharya 2021).

The percentage of explained variance *EV* is calculated for each value of *K* chosen clusters as follows:

$$EV_j = \frac{\sum_{i=1}^{j}\left(E_i - E_{i+1}\right)}{\Delta E_{max}} j = 1, 2, \ldots, K - 1, \tag{3}$$

where ΔE_{max} corresponds to the *E* deviation between 1 and the highest *K* among those analysed. As the number of clusters increases, *EV* will also increase, as more of the total variance is 'explained' by the clustering. The optimal *K* value is typically chosen to be the one corresponding to 90% or 95% of explained variance (Thorndike 1953).

The silhouette coefficient is an internal cluster validation that evaluates the clustering result based on the data clustering itself. It measures how well each object lies within its cluster, providing insight into the clustering quality and separation between clusters. The silhouette coefficient ($s\,[i]$) for each point is defined as follows (Aranganayagi and Thangavel 2007):

$$s(i) = \frac{b(i) - a(i)}{max\{a(i), b(i)\}}, \quad (4)$$

where $a(i)$ is the average distance between data i and all other points belonging to the same cluster and $b(i)$ is the smallest average distance of data i from all data belonging to the other clusters (Jain et al. 1999). By summing the silhouette coefficients of all the samples and dividing by the total number of data, an average coefficient is obtained, ranging in the interval $[-1, +1]$. An average silhouette score with a value equal to or close to $+1$ means that the group is characterized by maximum cohesion and data separation; a value close to or equal to -1 means minimal data cohesion and separation. Therefore, the *K*-best suggested by silhouette is the one corresponding to the average coefficient value closest to unity (Shahapure and Nicholas 2020).

Here, the cluster analysis was performed by using software packages available in the Statistics and Machine Learning Toolbox of MATLAB.

4 | Results

The results obtained from elbow and silhouette validation methods reveal distinct outcomes in both the number of clusters and their interpretability (Table 3).

The elbow method suggests between six to eight clusters for different frequencies and areas, particularly when applying a 90% or 95% explained variance threshold. However, this approach can lead to excessive detail and a large number of groups that do not effectively represent the geological or archaeological features, due to the area's inherent homogeneity. In contrast, the silhouette coefficient recommends a smaller *K*-best value, typically around two to three clusters. This smaller number of clusters captures the low lithological heterogeneity of the study area while accommodating significant variations in geophysical properties, such as magnetic susceptibility and electrical resistivity.

Furthermore, the silhouette analysis demonstrates greater consistency across different frequencies, maintaining a constant number of clusters regardless of frequency changes, with only variations in data volume within each cluster. Conversely, the elbow method shows fluctuations in cluster numbers with frequency changes, resulting in variability in proposed *K* values and data distribution among clusters.

Given these insights, it is inferred that the *K*-best value suggested by the silhouette coefficient provides a more meaningful partitioning of the dataset. Figure 5 illustrates the cluster analysis results in the parameter space for both 5- and 10-kHz acquisition frequencies. The retrieved clusters were categorized into four groups based on the range of variations of the EM components, enhancing the understanding and interpretation of the data. Figure 6 shows the results of the clusters analysis into the real space.

It is worth noting that the clusters identified in the parameter space, when mapped back to real space, illuminate contiguous areas and do not end up illuminating random pixels on the maps. This indicates that the employed clustering methodology is robust and effective. It also demonstrates that the parameters used for clustering are capturing meaningful spatial patterns rather than noise or outliers. This enhances the credibility of the analysis and suggests that the underlying data has a coherent structure.

5 | Discussion

The interpretation of the retrieved clusters is based on the LIN condition, which considers the in-phase component to be directly proportional to magnetic susceptibility and the quadrature component to be directly proportional to apparent electrical conductivity. Using archaeological and geological knowledge of the area, the four clusters were divided into two main groups:

- Natural background: characterized by low susceptibility values with low-to-medium conductivity (Cluster 2) and low susceptibility values with high conductivity (Cluster 3);
- Areas of Archaeological Interest (AAI): characterized by high magnetic susceptibility with low conductivity (Cluster 1) and high magnetic susceptibility with high conductivity (Cluster 4).

Cluster 2 (green in Figures 5 and 6) exhibits an average conductivity range for all meshes between 3 and 25 $mS\,m^{-1}$, with in-phase component values never exceeding 0.02 ppt, suggesting

TABLE 3 | *K_best* values from elbow and silhouette methods for the different meshes and acquisition frequencies.

Acquisition frequency	Mesh	*K*-best elbow method (explained variance 90%)	*K*-best elbow method (explained variance 95%)	*K*-best silhouette coefficient
5 kHz	M1	6	8	3
	M2	7	8	3
	M3	5	7	2
10 kHz	M1	6	7	3
	M2	7	7	3
	M3	6	8	2

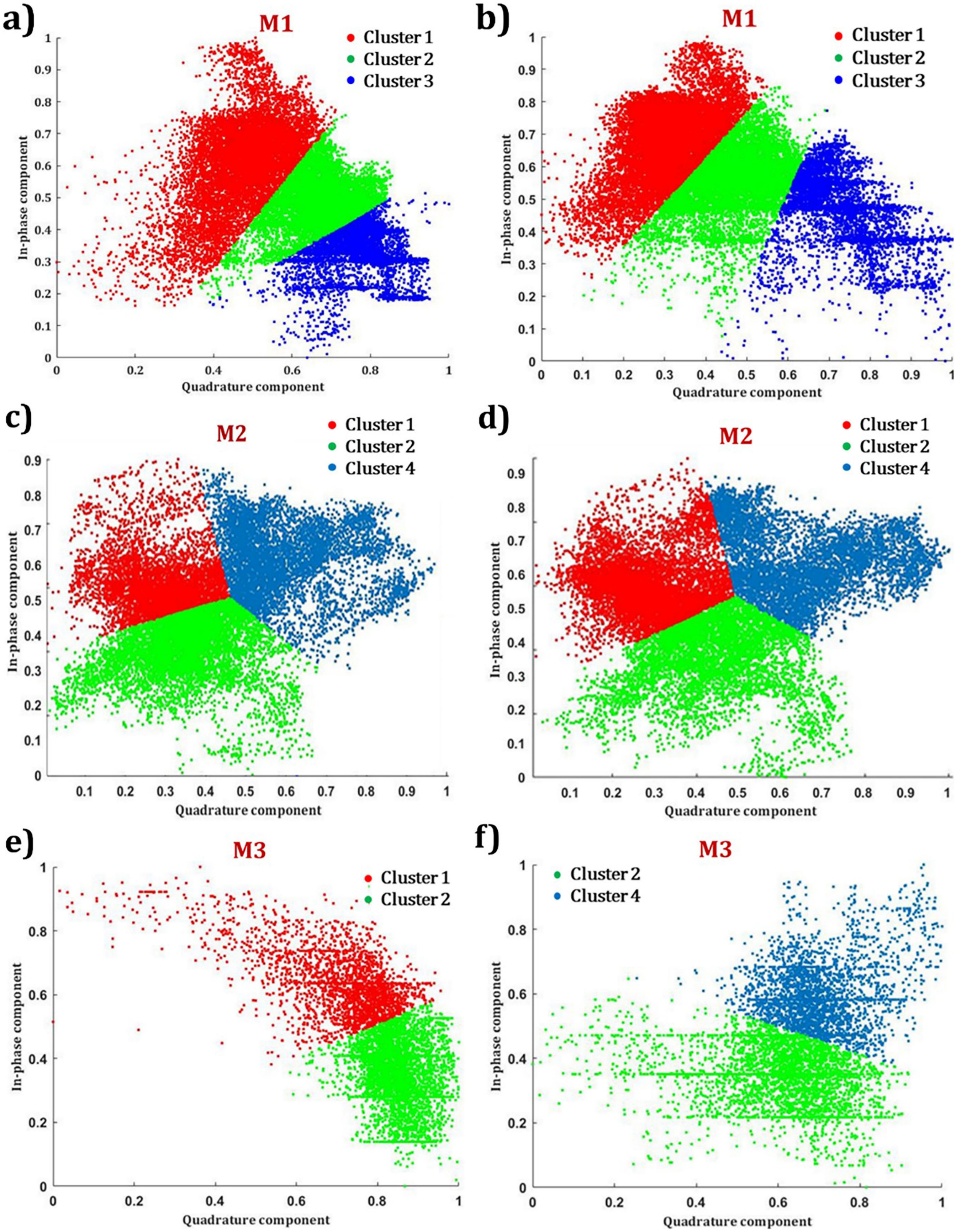

FIGURE 5 | Results of cluster analysis of EM normalized data based on silhouette coefficients. (a) M1 at $F = 5\,\text{kHz}$; (b) M1 at $F = 10\,\text{kHz}$; (c) M2 at $F = 5\,\text{kHz}$; (d) M2 at $F = 10\,\text{kHz}$; (e) M3 at $F = 5\,\text{kHz}$; (f) M3 at $F = 10\,\text{kHz}$.

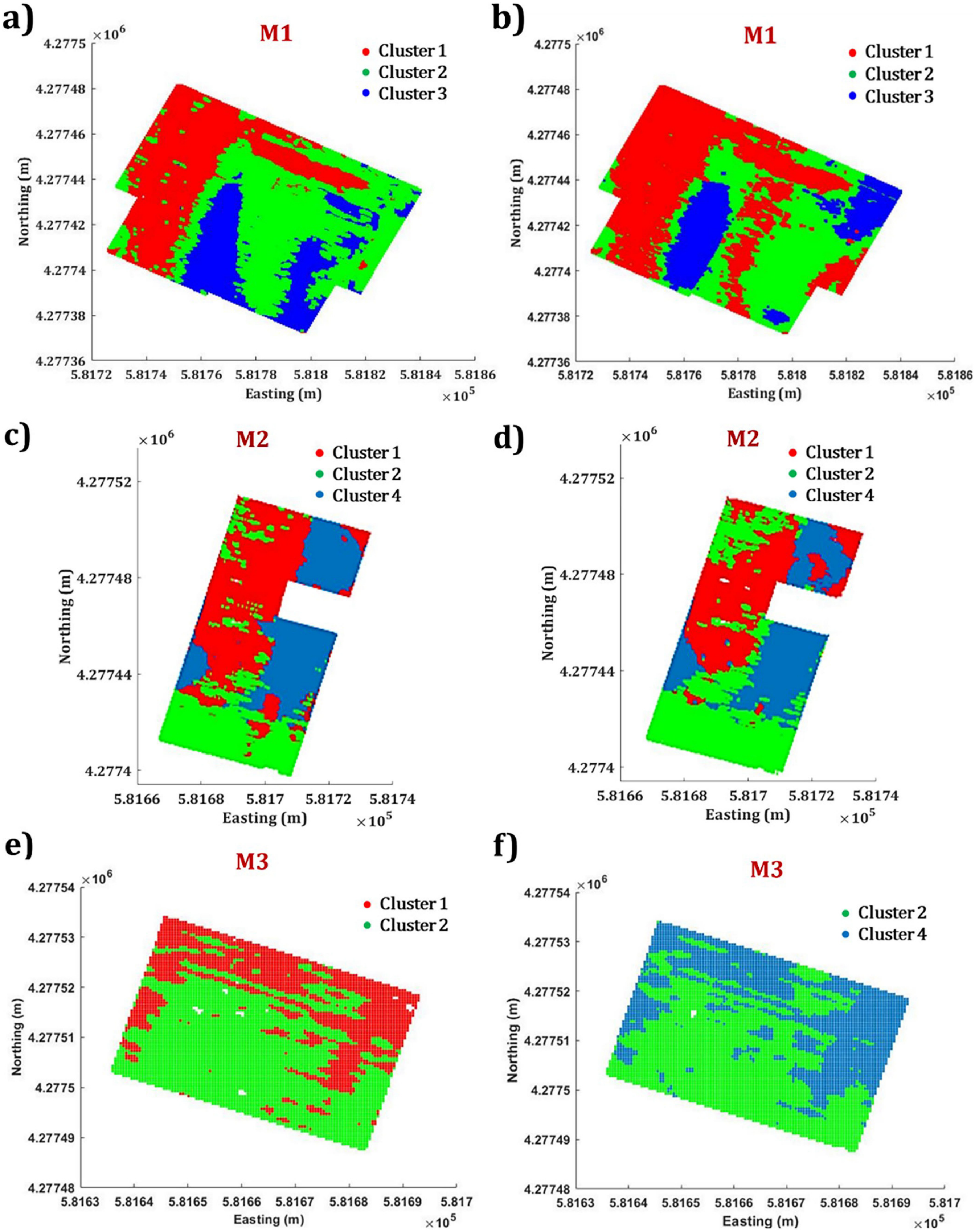

FIGURE 6 | Integrated maps of the EM components of the investigated area, corresponding to the clustering results shown in Figure 5. (a) M1 at $F = 5$ kHz; (b) M1 at $F = 10$ kHz; (c) M2 at $F = 5$ kHz; (d) M2 at $F = 10$ kHz; (e) M3 at $F = 5$ kHz; (f) M3 at F = 10 kHz.

compatibility with a sandstone background. Similarly, Cluster 3 (blue in Figures 5 and 6) is interpreted as a natural background. It exhibits a susceptibility range similar to Cluster 2, but with a slightly higher maximum conductivity, reaching approximately 35 mS m^{-1}. This modest difference in electrical conductivity may be explained by the presence of areas characterized by sandstone with a slightly higher grain size and/or saturation level.

Cluster 1 (red in Figures 5 and 6) has lower electrical conductivity compared to Cluster 2, peaking at around 20 mS m^{-1}, that is, relatively low. Furthermore, the values of the in-phase component are relatively high, up to approximately 0.023 ppt, implying high magnetic susceptibility values. These characteristics suggest that the materials in Cluster 1 may be more compact and more magnetic than surrounding sandstone. As mentioned above, this may indicate the presence of building materials such as bricks, which are commonly used in the construction of walls and roads. The indigo Cluster 4 could be related to the presence of small and sparse metallic materials, such as iron and bronze objects, both representative of the two periods of activity of the Torre Galli site. These materials exhibit relatively good magnetic properties (in-phase component of about 0.023 ppt) and electrical conductivity (up to 37 mS m^{-1}) (e.g., Dionne et al. 2011) higher than the surrounding environment.

Figure 6 reveals a clear spatial organization of clusters, as well as a distinct distribution of these clusters based on their operating frequencies. In mesh M1, the clusters of archaeological interest characterized by high magnetic susceptibility and low electrical conductivity values (red clusters in Figure 6a,b) are found in the northern and western sectors at 5 kHz (Figure 6a), whereas at 10 kHz, another area of interest in red appears in the central sector (Figure 6b). This has an elongated shape and limits a more conductive zone (Cluster 3). In mesh M2, the areas associated with the red clusters (Figure 6c,d) are localized essentially in the western sector for both the operational frequencies, whereas in M3, they appear in the northern sector only at 5 kHz (Figure 6e). Additionally, the maps indicate that regions of archaeological significance, marked by both relatively high susceptibility and elevated electrical conductivity, are more likely to be located in M2 and possibly in M3 (Figure 6c,d,f).

To validate the clustering results, a comparison was made with the outcome of a magnetic survey carried out in the same area by Cella and Fedi (2015), which analysed magnetic data at multiple scales.

The authors considered the pole reduced map of vertical gradient data (Figure 7a) and then applied the enhanced horizontal derivative (EHD) method (Fedi and Florio 2001) to outline the lateral boundaries of sources (Figure 7b). This method facilitated the identification of areas with varying magnetization. The magnetic data outcomes supported the archaeologists' hypotheses regarding a defence zone, leading to targeted excavations at M1 and M2, where remains of two ditches were uncovered, corresponding to magnetic maxima t12 and t17 (Figure 7b).

In Figure 7c,d, Clusters 1 and 4 (AAI clusters) are overlaid on the magnetic vertical gradient map, revealing a strong correlation between these clusters and significant magnetic anomalies.

Clusters 1 and 4 were also overlapped to EHD maps (Figure 7e,f). This comparison shows that all AAI clusters include magnetic maxima. It is noted that at 5 kHz, they also include the locations of trench t12 (width of 2.5 m) and trench t17 (width less than 2 m). Differences can be observed between the integrated EM maps at the two different acquisition frequencies. A notable distinction is the elongated anomalous area in the central-eastern sector of M1. These EHD anomalies (t21, formed by a pair of parallel alignments, and t22) fall within the red cluster area on the 10-kHz frequency map (Figure 7f) but not on the 5-kHz map (Figure 7e).

This discrepancy may be attributed to the ancient topography of the investigation area, which is not as regular and flat as it is today. This irregular terrain likely influenced the construction of defence walls and roads at varying levels, with some features located at greater depths.

Another difference is observed in M3, where electrical conductivity varies significantly with frequency. Given the lack of geological evidence for a shallow lithological change, the existence of subhorizontal layers is inferred. These layers may show varying gradations of erosion and compaction, potentially affecting saturation degrees or containing different types of archaeological material. However, these hypotheses remain assumptions that only excavation can confirm.

The strong correlation between the magnetic analysis results and these findings underscores that a key factor in distinguishing archaeological features from the natural environment at the Torre Galli site is the contrast in magnetic susceptibility between the two sources. Shallow soils, formed from weathered arenaceous bedrock with a predominant carbonate fraction, are expected to exhibit very low susceptibility. In contrast, materials used in the discovered structures, such as bricks for walls and road paving, show moderate susceptibility slightly higher than the background.

Compared to the magnetic method, this new representation of the EM data allows simultaneous examination of susceptibility and conductivity. This enabled to categorize highly magnetic regions into two subgroups based on conductivity. More specifically, the two AAI groups that exhibit similar susceptibility ranges were divided into (i) a subgroup showing low electrical conductivity (such as bricks) and (ii) a subgroup with high electrical conductivity (such as accumulations of bronze/iron materials). Thus, the proposed approach provides archaeologists with insights into different potential target types across areas of major archaeological interest, identifying zones characterized by varying relationships in electrical and magnetic properties. Additionally, this approach enables the recognition of different area characteristics as the operating frequency changes, a distinction that has not been observed with traditional methods, as noted by Cella and Fedi (2015).

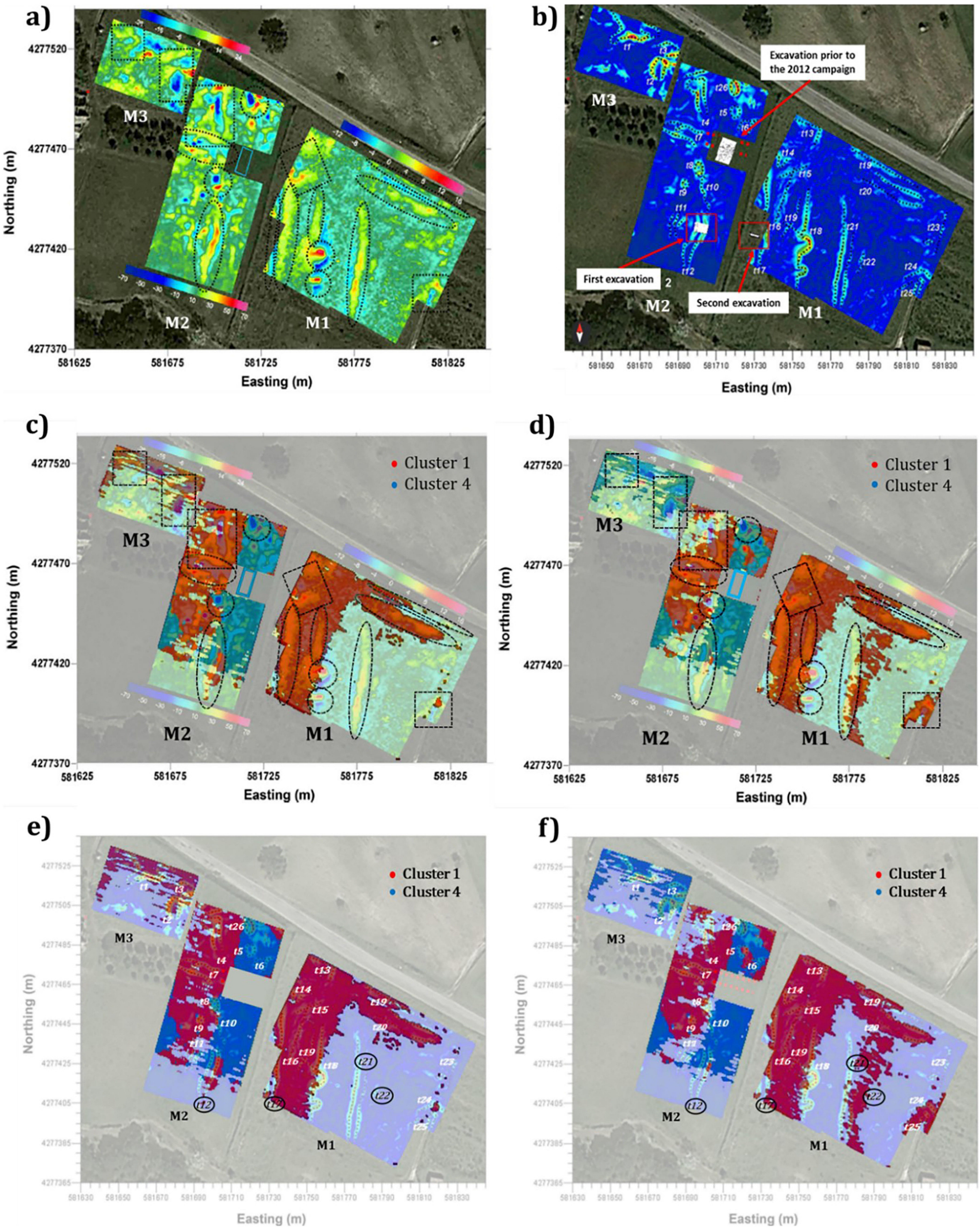

FIGURE 7 | Spatial distribution of magnetic data and AAI clusters: (a) pole-reduced vertical-gradient magnetic data (ellipses: linear anomalies; rectangles: 'box-shaped' anomalies; and circles: dipolar anomalies) and (b) EHD map of magnetic data (modified after Cella and Fedi 2015). (c, d) Overlap of pole-reduced vertical-gradient magnetic data with AAI clusters for 5 and 10 kHz, respectively. (e, f) Overlap of EHD of magnetic data with AAI clusters for 5 and 10 kHz, respectively.

6 | Conclusions

This study employed the *K*-means clustering algorithm to combine the in-phase and quadrature components of the electromagnetic (EM) field. This approach enabled the creation of integrated EM maps, offering a comprehensive view of the apparent electrical conductivity and magnetic susceptibility of the surveyed area. The proposed innovative visualization allowed the identification of spatial regions defined by specific intervals of these properties, highlighting areas that share similar characteristics, regardless of their distance apart. This automatic correlation significantly reduces interpreter subjectivity, moving beyond simple visual inspection.

The integrated maps have facilitated the automatic identification of key areas with potential archaeological interest, characterized by high susceptibility values and variable electrical conductivity. After classifying these areas, they were overlaid with results from previous magnetic analyses to validate the findings. This comparison revealed that all features identified through magnetic methods were also captured in the FDEM analysis, although the EHD method (see Figure 7b) provided more detailed information due to careful weight selection and extensive data processing. In contrast, mapping EM clusters allows for a rapid assessment to identify areas of greatest interest, highlighting different characteristics as the operating frequency varies, significantly reducing both the extent of land subject to further geophysical analyses and/or excavation and associated costs.

The advanced analysis performed in the area suggests that archaeologists should prioritize future studies in the regions covered by Cluster 1 (red) (Figure 7) if they intend to excavate buried structures characterized by higher resistivity, such as roads and/or walls. Conversely, if they are interested in examining more conductive objects like iron/bronze tools and weapons, a more detailed investigation of the areas marked by Cluster 4 (indigo) is advisable (Figure 7).

However, users should use caution when drawing conclusions without a well-understood geological context or sufficient archaeological knowledge of the site. Failing to consider these factors may lead to increased time and costs rather than savings.

Future studies will involve conducting a multivariate analysis that incorporates spatial coordinates to evaluate whether expanding the dimensionality of the parameter space leads to a consistent improvement in delineating areas of archaeological interest.

Acknowledgements

We wish to thank Prof. Maurizio Fedi for sharing his years of experience with us during the discussion phase of this work. We thank two anonymous reviewers for their suggestions, which helped us improve the manuscript. Open access publishing facilitated by Universita degli Studi di Napoli Federico II, as part of the Wiley - CRUI-CARE agreement.

Conflicts of Interest

The authors declare no conflicts of interest.

Data Availability Statement

The data that support the findings of this study are available on request from the corresponding author. The data are not publicly available due to privacy or ethical restrictions.

References

Abbate, S. 2014. "L'armamento del Guerriero in Calabria Durante la Prima età del Ferro, nel Quadro dell'Italia Meridionale." *Catalogo Cosenza* 2014: 77–84.

Ambrosino, M., S. Albanese, B. De Vivo, et al. 2022. "Identification of Rare Earth Elements (REEs) Distribution Patterns in the Soils of Campania Region (Italy) Using Compositional and Multivariate Data Analysis." *Journal of Geochemical Exploration* 243: 107112. https://doi.org/10.1016/j.gexplo.2022.107112.

Ambrosino, M., Z. El-Saadani, A. A. Khatita, W. Mingqi, J. Palarea-Albaladejo, and D. Cicchella. 2023. "Geochemical Speciation, Ecological Risk and Assessment of Main Sources of Potentially Toxic Elements (PTEs) in Stream Sediments From Nile River in Egypt." *Water* 15, no. 13: 2308. https://doi.org/10.3390/w15132308.

Ambrosino, M., J. Palarea-Albaladejo, S. Albanese, and D. Cicchella. 2024. "Mapping Geochemical Domains Using Stream Sediment Geochemistry: An Approach Based on Compositional Indicators in the Volturno River Basin (South Italy)." *Journal of Geochemical Exploration* 265: 107545. https://doi.org/10.1016/j.gexplo.2024.107545.

Aranganayagi, S., and K. Thangavel. 2007. "Clustering Categorical Data Using Silhouette Coefficient as a Relocating Measure." In *International Conference on Computational Intelligence and Multimedia Applications (ICCIMA 2007)*, vol. 2, 13–17. Sivakasi, India: IEEE. https://doi.org/10.1109/ICCIMA.2007.328.

Benech, C., M. Dabas, F. X. Simon, A. Tabbagh, and J. Thiesson. 2016. "Interpretation of Shallow Electromagnetic Instruments Resistivity and Magnetic Susceptibility Measurements Using Rapid 1D/3D Inversion." *Geophysics* 81, no. 2: E103–E112. https://doi.org/10.1190/geo2014-0549.1.

Benelli, M. V. 2012. "TORRE GALLI. Bibliografia Topografica Della Colonizzazione Greca in Italia e Nelle Isole Tirreniche." *Rivista di Studi Classici* 21, no. 1: 23–33.

Bernardinetti, S., and P. P. G. Bruno. 2019. "The Hydrothermal System of Solfatara Crater (Campi Flegrei, Italy) Inferred From Machine Learning Algorithms." *Frontiers in Earth Science* 7: 286. https://doi.org/10.3389/feart.2019.00286.

Bettelli, M., and L. Vagnetti. 2019. *Southern Italy. A Companion to the Archaeology of Early Greece and the Mediterranean*, 1261–1286. Wiley. https://doi.org/10.1002/9781118769966.ch52.

Bhattacharya, S. 2021. *A Primer on Machine Learning in Subsurface Geosciences*. Vol. 1, 1–172. Springer.

Bianco, L., M. La Manna, V. Russo, and M. Fedi. 2024. "Magnetic and GPR Data Modelling via Multiscale Methods in San Pietro in Crapolla Abbey, Massa Lubrense (Naples)." *Archaeological Prospection* 31, no. 2: 139–147. https://doi.org/10.1002/arp.1936.

Boschi, F. 2020. *Archeologia Senza Scavo. Geofisica e Indagini Non Invasive*. Italia: Bononia University Press.

Calcaterra, D., and M. Parise. 2010. "Weathering in the Crystalline Rocks of Calabria, Italy, and Relationships to Landslides." *Geological Society, London, Engineering Geology Special Publications* 23, no. 1: 105–130. https://doi.org/10.1144/EGSP23.7.

Carrara, E., M. T. Carrozzo, M. Fedi, et al. 2001. "Resistivity and Radar Surveys at the Archaeological Site of Ercolano." *Journal of Environmental and Engineering Geophysics* 6, no. 3: 123–132. https://doi.org/10.4133/JEEG6.3.123.

Casas, A., P. Castanyer, M. Himi, et al. 2022. "Frequency Domain Electromagnetic Mapping for Delineating Subsurface Structures Related to the Historical Port of Emporiae." *Archaeological Prospection* 29, no. 1: 33–43. https://doi.org/10.1002/arp.1834.

Cella, F., and M. Fedi. 2015. "High-Resolution Geophysical 3D Imaging for Archaeology by Magnetic and EM Data: The Case of the Iron Age Settlement of Torre Galli, Southern Italy." *Surveys in Geophysics* 36, no. 6: 831–850. https://doi.org/10.1007/s10712-015-9341-3.

Cella, F., V. Paoletti, G. Florio, and M. Fedi. 2015. "Characterizing Elements of Urban Planning in Magna Graecia Using Geophysical Techniques: The Case of Tirena (Southern Italy)." *Archaeological Prospection* 22, no. 3: 207–219. https://doi.org/10.1002/arp.1507.

Christiansen, A. V., J. B. Pedersen, E. Auken, N. E. Søe, M. K. Holst, and S. M. Kristiansen. 2016. "Improved Geoarchaeological Mapping With Electromagnetic Induction Instruments From Dedicated Processing and Inversion." *Remote Sensing* 8, no. 12: 1022. https://doi.org/10.3390/rs8121022.

Cicchella, D., M. Ambrosino, A. Gramazio, et al. 2022. "Using Multivariate Compositional Data Analysis (CoDA) and Clustering to Establish Geochemical Backgrounds in Stream Sediments of an Onshore Oil Deposits Area. The Agri River Basin (Italy) Case Study." *Journal of Geochemical Exploration* 238: 107012. https://doi.org/10.1016/j.gexplo.2022.107012.

Cozzolino, M., E. Di Giovanni, P. Mauriello, S. Piro, and D. Zamuner. 2018. *Geophysical Methods for Cultural Heritage Management*. Springer Geophys. https://doi.org/10.1007/978-3-319-74790-3.

Cutaneo, C., A. Vitale, and M. Fedi. 2023. "Unsupervised Boundary Analysis of Potential Field Data: A Machine Learning Method." *Geophysics* 88, no. 3: G57–G65. https://doi.org/10.1190/geo2022-0146.1.

De Smedt, P., T. Saey, A. Lehouck, et al. 2013. "Exploring the Potential of Multi-Receiver EMI Survey for Geoarchaeological Prospection: A 90 ha Dataset." *Geoderma* 199: 30–36. https://doi.org/10.1016/j.geoderma.2012.07.019.

Deiana, R., G. P. Deidda, E. D. Cusí, P. van Dommelen, and A. Stiglitz. 2022. "FDEM and ERT Measurements for Archaeological Prospections at Nuraghe S'urachi (West-Central Sardinia)." *Archaeological Prospection* 29, no. 1: 69–86. https://doi.org/10.1002/arp.1838.

Deidda, G. P., P. Diaz de Alba, C. Fenu, G. Lovicu, and G. Rodriguez. 2020. "FDEMtools: A MATLAB Package for FDEM Data Inversion." *Numerical Algorithms* 84: 1313–1327. https://doi.org/10.1007/s11075-019-00843-2.

Desgraupes, B. 2013. "Clustering Indices." *University of Paris Ouest-Lab Modal'x* 1, no. 1: 34.

Di Maio, R., M. La Manna, E. Piegari, A. Zara, and J. Bonetto. 2018. "Reconstruction of a Mediterranean Coast Archaeological Site by Integration of Geophysical and Archaeological Data: The Eastern District of the Ancient City of Nora (Sardinia, Italy)." *Journal of Archaeological Science: Reports* 20: 230–238. https://doi.org/10.1016/j.jasrep.2018.05.003.

Dionne, C. A., J. J. Schultz, R. A. Murdock II, and S. A. Smith. 2011. "Detecting Buried Metallic Weapons in a Controlled Setting Using a Conductivity Meter." *Forensic Science International* 208, no. 1–3: 18–24. https://doi.org/10.1016/j.forsciint.2010.10.019.

El-Qady, G., and M. Metwaly. 2018. *Archaeogeophysics: State of the Art and Case Studies*. Springer.

Fedi, M., F. Cella, G. Florio, M. La Manna, and V. Paoletti. 2017. *Geomagnetometry for Archaeology. Sensing the Past: From Artifact to Historical Site*, 203–230. Springer. https://doi.org/10.1007/978-3-319-50518-3_10.

Fedi, M., and G. Florio. 2001. "Detection of Potential Fields Source Boundaries by Enhanced Horizontal Derivative Method." *Geophysical Prospecting* 49, no. 1: 40–58. https://doi.org/10.1046/j.1365-2478.2001.00235.x.

Florio, G., F. Cella, L. Speranza, R. Castaldo, R. Pierobon Benoit, and R. Palermo. 2019. "Multiscale Techniques for 3D Imaging of Magnetic Data for Archaeo-Geophysical Investigations in the Middle East: The Case of Tell Barri (Syria)." *Archaeological Prospection* 26, no. 4: 379–395. https://doi.org/10.1002/arp.1751.

Florio, G., and D. Lo Re. 2018. "Terracing of Potential Fields by Clustering Methods." *Geophysics* 83, no. 4: G47–G58. https://doi.org/10.1190/geo2017-0140.1.

Fraser, D. C. 1972. "A New Multicoil Aerial Electromagnetic Prospecting System." *Geophysics* 37, no. 3: 518–537. https://doi.org/10.1190/1.1440277.

Gaffney, C. F., J. Gater, and S. Ovenden. 2002. *The Use of Geophysical Techniques in Archaeological Evaluations*. Vol. 6. Reading, UK: Institute of Field Archaeologists.

Gramigna, P., A. Guido, A. Mastandrea, and F. Russo. 2008. "The Paleontological Site of Cessaniti: A Window on a Coastal Marine Environment of Seven Million Years Ago (Southern Calabria, Italy)." *Geologica Romana* 41: 25–34.

Grassi, S., G. Morreale, R. Lanteri, et al. 2023. "Integration of Geophysical Survey Data for the Identification of New Archaeological Remains in the Subsoil of the Akrai Greek Site (Sicily, Italy)." *Heritage* 6, no. 2: 979–992. https://doi.org/10.3390/heritage6020055.

Ietto, A., and F. Ietto. 2004. "Age and History of the Weathering of Granitoids in Southern Calabria (Italy)." *Geografia Fisica e Dinamica del Quaternario* 27: 37–45.

Jain, A. K., M. N. Murty, and P. J. Flynn. 1999. "Data Clustering: A Review." *ACM Computing Surveys* 31, no. 3: 264–323. https://doi.org/10.1145/331499.331504.

La Genière, J. 1964. "Note sur la Chronologie des nécropoles de Torre Galli et Canale-Janchina." *MEFR(A)* LXXVI: 7–23.

Martorana, R., P. Capizzi, A. Pisciotta, S. Scudero, and C. Bottari. 2023. "An Overview of Geophysical Techniques and Their Potential Suitability for Archaeological Studies." *Heritage* 6, no. 3: 2886–2927. https://doi.org/10.3390/heritage6030154.

McNeill, J. D. 1980. *Electromagnetic Terrain Conductivity Measurement at Low Induction Numbers*. Technical Note TN-6, 1–15. Mississauga, ON, Canada: Geonics Ltd.

Milo, P., M. Vágner, T. Tencer, and I. Murín. 2022. "Application of Geophysical Methods in Archaeological Survey of Early Medieval Fortifications." *Remote Sensing* 14, no. 10: 2471. https://doi.org/10.3390/rs14102471.

Modabberi, S., M. Tashakor, N. Rajabian, et al. 2023. "Characterization and Chemical Fractionation of Potentially Toxic Elements in Soils of a Pre-Mining Mineralized Area; an Evaluation of Mobility and Environmental Risk." *Environmental Geochemistry and Health* 45, no. 7: 4795–4815. https://doi.org/10.1007/s10653-023-01537-4.

Murphy, K. P. 2012. *Machine Learning: A Probabilistic Perspective*. Cambridge, Massachusetts: MIT Press.

Narciso, J., E. van de Vijver, and L. Azevedo. 2025. "Geostatistical Inversion of Frequency-Domain Electromagnetic Data for Near-Surface Modelling." *Geophysics* 90, no. 1: E13–E27. https://doi.org/10.1190/geo2023-0358.1.

Nicotera, P. 1959. "Rilevamento Geologico del Versante Settentrionale del Monte Poro (Calabria)." *Memorie e Note dell'Istituto di Geologia Applicata di Napoli* 7: 1–92.

Orsi, P. 1926. *Le Necropoli Preelleniche Calabresi di Torre Galli e di Canale*. Ianchina, Patariti, Bardi.

Orsi, P. 2004. *Le Necropoli Preelleniche Calabresi. Torre Galli, Canale, Ianchina, Patariti*. FPE-Franco Pancallo Editore ISBN 8864561323, 9788864561325.

Pacciarelli, M. 1999. *Torre Galli. La Necropoli Della Prima eta' del Ferro (scavi di Paolo Orsi 1922-23)*. Rubbettino Editore, Iraceb 8872847257.

Pacciarelli, M., C. Iaia, and I. Matarese. 2017. "Torre Galli: Le Campagne di Scavo 2012-2013." In *Centri Fortificati Indigeni Della Calabria Dalla Protostoria All'età Ellenistica*, 337–350. Naus.

Paoletti, V., M. La Manna, A. Capozzoli, M. Mercurio, M. Zinni, and A. Naso. 2024. "GPR Survey at the Etruscan Necropolis of Sasso Pinzuto, Tuscania (Central Italy)." *Journal of Archaeological Science: Reports* 60: 104833. https://doi.org/10.1016/j.jasrep.2024.104833.

Paoletti, V., M. Secomandi, M. Piromallo, F. Giordano, M. Fedi, and A. Rapolla. 2005. "Magnetic Survey at the Submerged Archaeological Site of Baia, Naples, Southern Italy." *Archaeological Prospection* 12, no. 1: 51–59. https://doi.org/10.1002/arp.243.

Piegari, E., G. De Donno, D. Melegari, and V. Paoletti. 2023. "A Machine Learning-Based Approach for Mapping Leachate Contamination Using Geoelectrical Methods." *Waste Management* 157: 121–129. https://doi.org/10.1016/j.wasman.2022.12.015.

Piro, S. 2008. "Introduction to Geophysics for Archaeology." In *Seeing, the Unseen. Geophysics and Landscape Archaeology*, 53–92. CRC Press.

Rao, A., P. Gramigna, and C. Neri. 2007. "Aspetti Sedimentologici e Biostratigrafici Della Sezione Neogenica di Piscopio Nell'area di M.te Poro, Vibo Valentia (Calabria)." *Geologica Romana* 40: 147–161.

Reynolds, J. M. 2011. *An Introduction to Applied and Environmental Geophysics*. Second ed, 712. Chichester: John Wiley & Sons.

Rizzo, E., R. Dubbini, J. Clementi, et al. 2023. "Geomagnetic and FDEM Methods in the Roman Archaeological Site of Bocca Delle Menate (Comacchio, Italy)." *Heritage* 6, no. 2: 1698–1712. https://doi.org/10.3390/heritage6020090.

Saey, T., P. de Smedt, M. Monirul Islam, et al. 2012. "Depth Slicing of Multi-Receiver EMI Measurements to Enhance the Delineation of Contrasting Subsoil Features." *Geoderma* 189–190: 514–521. https://doi.org/10.1016/j.geoderma.2012.06.010.

Sea, C. D., and E. G. Ernenwein. 2021. "Frequency Domain Electromagnetic Induction: An Efficient Method for Investigating Fort Ancient Village Dynamics." *Archaeological Prospection* 28, no. 1: 73–87. https://doi.org/10.1002/arp.1798.

Shahapure, K. R., and C. Nicholas. 2020. "Cluster Quality Analysis Using Silhouette Score." In *2020 IEEE 7th International Conference on Data Science and Advanced Analytics (DSAA)*, 747–748. IEEE. https://doi.org/10.1109/DSAA49011.2020.00096.

Simon, F. X., A. Sarris, J. Thiesson, and A. Tabbagh. 2015. "Mapping of Quadrature Magnetic Susceptibility/Magnetic Viscosity of Soils by Using Multi-Frequency EMI." *Applied Geophysics* 12, no. 0: 36–47. https://doi.org/10.1016/j.jappgeo.2015.06.007.

Soupios, P., N. Papadopoulos, and A. Sarris. 2013. "Reconstructing Concealed Cultural Remains Through Integrated Geophysical Tomographic Methods." *Bulletin of the Geological Society of Greece* 47, no. 3: 1260–1268. https://doi.org/10.12681/bgsg.10900.

Tabbagh, A. 1986. "Applications and Advantages of the Slingram Electromagnetic Method for Archaeological Prospecting." *Geophysics* 51, no. 3: 576–584. https://doi.org/10.1190/1.1442112.

Thorndike, R. L. 1953. "Who Belongs in the Family?" *Psychometrika* 18, no. 4: 267–276. https://doi.org/10.1007/BF02289263.

Tortorici, G., M. Bianca, G. De Guidi, C. Monaco, and L. Tortorici. 2003. "Fault Activity and Marine Terracing in the Capo Vaticano Area (Southern Calabria) During the Middle and Late Quaternary." *Quaternary International* 102: 269–278. https://doi.org/10.1016/S1040-6182(02)00107-6.

Wait, J. R. 1955. "Mutual Electromagnetic Coupling of Loops Over a Homogeneous Ground." *Geophysics* 20, no. 3: 630–637. https://doi.org/10.1190/1.1438167.

Won, I. J., and H. Huang. 2004. "Magnetometers and Electromagnetometers." *Leading Edge* 23: 448–451. https://doi.org/10.1190/1.1756834.